

Received November 25, 2020, accepted December 10, 2020, date of publication December 23, 2020, date of current version January 11, 2021.

Digital Object Identifier 10.1109/ACCESS.2020.3046713

Quantitative Design and Implementation of an Induction Cooker for a Copper Pan

MING-SHI HUANG¹, (Member, IEEE),
CHIH-CHIA LIAO¹, (Graduate Student Member, IEEE),
ZHENG-FENG LI¹, (Graduate Student Member, IEEE), ZHI-REN SHIH¹,
AND HSIU-WEN HSUEH²

¹Department of Electrical Engineering, National Taipei University of Technology, Taipei 10608, Taiwan

²Department of Industrial Education and Technology, National Changhua University of Education Jin De Campus, Changhua 500, Taiwan

Corresponding author: Ming-Shi Huang (mingshi.huang@gmail.com)

ABSTRACT The nonferromagnetic pans with a low equivalent resistance are desired to generate sufficient power for heating by larger eddy current. First, Maxwell 3D is used to estimate the equivalent heating resistance of a copper pan and select the optimal number of turns for a induction coil by Litz wire according to its size limitations and efficiency. Furthermore, the optimal resonant frequency is determined by maximizing the heating efficiency. Finally, the electric parameters are obtained to construct a simulation environment for the design of control strategies. A full-wave rectifier, buck converter, and half-bridge resonant converter are cascaded to construct the converter. Because of low equivalent resistance and high quality factor of the copper pan, a high slope ratio of the resonant current to the frequency is obtained. Therefore, the resonant converter is operated at a fixed switching frequency to reduce low-frequency oscillations of the resonant current. The buck converter is used to control the DC link voltage with third-harmonic injection, which enables heating power control, increases heating power and satisfies the standard, IEC-61000-3-2 Class A. Moreover, a resonant frequency estimator is developed to detect the resonant frequency for various positions of the pan on the induction coil to determine the optimal heating frequency. Finally, TMS320F28075-based converter with 100 A of peak resonant current is built. The heating effect and power loss on a copper pan is then measured, and the maximum heating efficiency is 69%. The measurement results verify the effectiveness of the proposed induction cooker and exhibits excellent agreement with the simulated results.

INDEX TERMS Nonferromagnetic pans, Maxwell 3D, half-bridge resonant converter, heating power control.

I. INTRODUCTION

Induction heating (IH) has become popular in domestic cooking because of its high efficiency, fast heating, accurate power control, and safety [1], [2]. Because induction cookers are flame-free, they are a convenient replacement for gas cooktops in tall buildings in earthquake-prone countries [3]. In induction cooking, a high-frequency magnetic flux is generated to induce high-frequency eddy current and hysteresis on a thin surface for heating a vessel. Conventional induction cookers consist of an AC–DC rectifier, a resonant converter, and an induction coil so that they can generate high-frequency magnetic flux and the coil with a pan acts as the resonant inductor of the resonant circuit [4]–[6]. Half-bridge series resonant converters are cost-effective circuits for IH and can

be modeled as RLC circuits [6], and the pan and induction coil are equivalent to the resistor and inductor of RLC circuits [7]. The electric parameters of the aforementioned converters depend on the pan material, operating frequency, temperature, flux saturation of ferromagnetic materials, and relative position of the coil and pan [7]–[11]. Because current converters for IH are voltage sources in principle, adjusting the impedance of the resonant tank by changing the operating frequency with 50% duty (VF) [12] is a popular method for controlling the heating power. However, VF control cannot provide a wide range of power levels [13]. Although pulse density modulation [14] and discontinuous conduction modes can provide low power, the current harmonics may induce EMI issue.

Although technologies for heating ferromagnetic pans have matured, limited research has been conducted on the heating of nonferromagnetic materials, such as copper and

The associate editor coordinating the review of this manuscript and approving it for publication was Bo Pu¹.

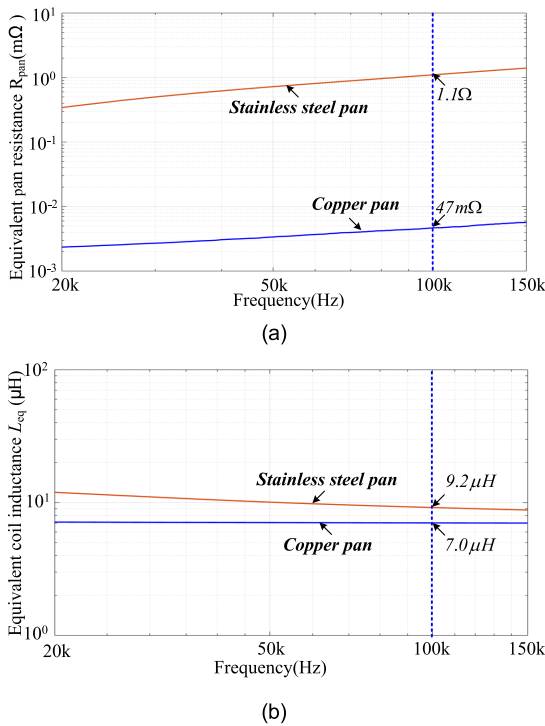


FIGURE 1. Resistance and inductance of nonferromagnetic and ferromagnetic pans on 14-cm-diameter induction coils measured using a WK 6500B impedance analyzer: (a) resistance; (b) inductance.

aluminum. Nonferromagnetic pans cannot be heated through conventional IH because of the following reasons. The heating mechanism in IH is eddy currents. Therefore, the low heating resistance [15], [16] of nonferromagnetic materials results in insufficient heat generation. Furthermore, IH operates with low efficiency if the resistances of the induction coil and nonferromagnetic pan become close due to improper design. Typically, the heating resistance of ferromagnetic pans is more than ten times that of nonferromagnetic pans. Fig. 1 displays the measured results of equivalent resistance of pan R_{pan} and equivalent coil inductance L_{eq} of the non-ferromagnetic (copper) and ferromagnetic (IH stainless) pans of the same size by an impedance analyzer without considering the flux saturation. The resistance of the copper pan used in this study was $47\text{ m}\Omega$, which is only 5% of the resistance of IH stainless pan at 100 kHz. Therefore, the current in the copper pan should be 4.8 times the current in the coil to yield the same heating power for IH stainless pans at 100 kHz. Table 1 displays the key characteristics of ferromagnetic and non-ferromagnetic materials for induction cooking, which includes R_{pan} , L_{eq} , change rate of inductance against frequency $\frac{\Delta L_{eq}}{\Delta f}$ and resonant current against frequency $\frac{\Delta i_{re}}{\Delta f}$.

Copper is an excellent conductor of heat, and copper pans are often used to heat sauces and dishes at strictly controlled temperatures. IH of nonferromagnetic pans can be achieved through various approaches, such as the use of an induction adapter, a thin slab [8], or a reducer plate [17], multiple induction coils [18], [19], and high current and high-frequency

TABLE 1. Characteristics of the pan materials.

Pan Materials	L_{eq}	$\frac{\Delta L_{eq}}{\Delta f}$	R_{eq}	$\frac{\Delta i_{re}}{\Delta f}$	Heating efficiency
Non-ferromagnetic	Small	Low	Small	High	Low
Ferromagnetic	Large	High	Large	Low	High

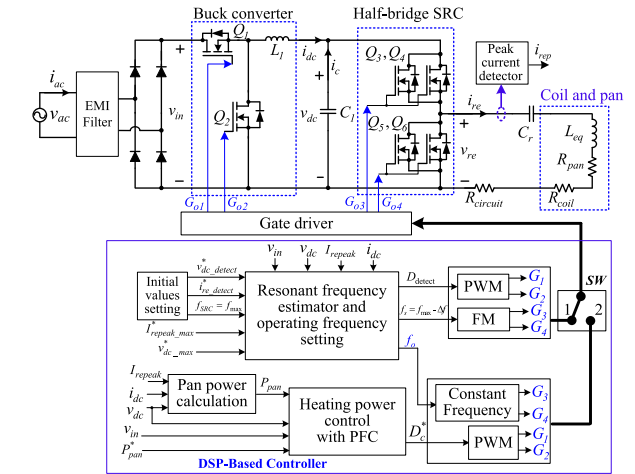


FIGURE 2. Proposed IH system for copper pans.

resonant converters [15], [20]–[22]. The first two methods involve heating the plate and then transferring the heat to nonferromagnetic pans. However, this approach poses a risk of scalding users. The effectiveness of IH depends on the shapes of both the plate surfaces and coils as well as the region coupled to the magnetic flux [23]. Although increasing the turns of the induction coil generates additional flux on the pan, the coil resistance also increases, which reduces the heating efficiency [7]. In [20], [21], the authors used a low switching frequency to generate a resonant current with a third-harmonic frequency close to the resonant frequency for achieving high heating power by changing the resonant capacitor. Because the method requires high DC link voltage, a time-sharing frequency-doubled resonant converter [22] is used for nonferromagnetic pans. In a previous study, a high-frequency transformer with a turns ratio of 17:3 is cascaded between a full-bridge circuit and a resonant tank to increase the load impedance for drastically reducing the MOSFET rated current [24].

The proposed IH system is illustrated in Fig. 2. The power stage mainly consists of a passive AC–DC rectifier, buck converter with synchronous rectifier control, and a half-bridge series resonant converter (HBSRC) in cascade. The buck converter is used to control the DC link voltage for achieving power control, increasing heating power, and satisfying the standard IEC-61000-3-2 Class A [25]. Therefore, the HBSRC operated at a fixed frequency to reduce low-frequency oscillations of the resonant current, which are caused by the insufficient resolution of the operating frequency. A resonant frequency estimator is proposed to determine the resonant frequency for various pan sizes and pan positions on the induction coil to obtain the optimal operation frequency before

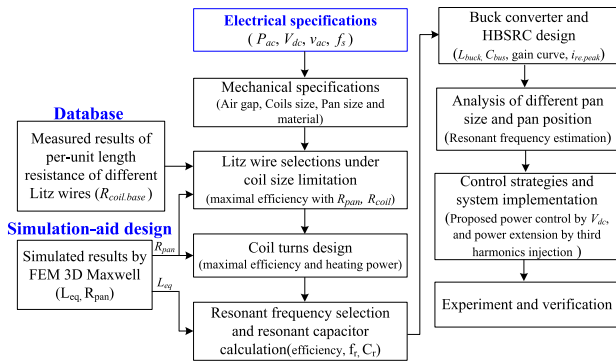


FIGURE 3. Design flowchart of the proposed IH system for copper pans.

heating and to improve safety. The proposed design procedure is displayed in Fig. 3. First, Maxwell 3D and MATLAB are used to design the induction coil and resonant frequency to maximize efficiency. Next, the HBSRC and buck converter are constructed for heating power control with a fixed switching operating frequency. The simulation results indicate that an induction coil made of a 0.05-mm and 3200-strand Litz wire is optimal for reducing the skin effect and enhancing efficiency. The frequency characteristics of the coil resistance are measured using an impedance analyzer. Finally, a DSP-based controller (TMS320F28075) is used for implementing the control methodologies. The simulation and experimental results revealed that the operating frequency and number of turns of the induction coil influenced the heating efficiency. Furthermore, the resonant inductance and equivalent heating resistance obtained for the proposed induction cooker by using power integration and the impedance analyzer exhibited excellent agreement with the corresponding simulations obtained using Maxwell 3D. The proposed control approaches of resonant frequency estimation and increasing heating power through third-harmonic injection are verified through experimental results.

This paper derived the design procedure by using simulated software for self-inductance, coupling factor, misalignment effects, and voltage gain in advance for the converter design to reach needed functions with higher efficiency.

II. OPTIMAL DESIGN OF AN IH SYSTEM THROUGH SIMULATION

The software-assisted procedure for designing an IH system is as follows. First, Ansys Maxwell 3D is used to analyze the eddy current heating phenomenon in the copper pan through electromagnetic induction. Then, a pan size is selected and as a nominal value, and the Litz wire is used as the induction coil. Moreover, the AC resistance of the coil is measured using an impedance analyzer. Furthermore, the number of turns of the induction coil and the operating frequency of IH are selected using Maxwell 3D to obtain high efficiency for the required specification. The equivalent heating resistance of the selected pan and the inductances of the induction coil with and without the pan are simulated by Maxwell 3D.

TABLE 2. Electrical specifications of proposed IH.

Parameter	Value
Pan material	Copper
Inner diameter of pan (mm)	180
Bottom diameter of pan (mm)	155
Diameter of coil (mm)	200
Rated input power (W)	650
Input ac RMS voltage (V)	110
DC link voltage (V)	35 – 70
Maximum resonant current (A)	50 – 100
Switching frequency of SRC (kHz)	132
Switching frequency of buck (kHz)	100
Buck inductor (μ H)	100
DC link capacitance (μ F)	33
Maximum efficiency (%)	69

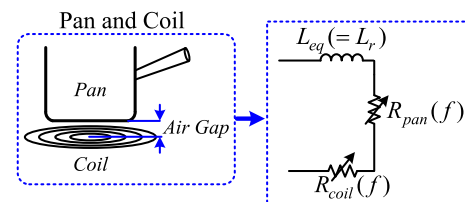


FIGURE 4. Equivalent circuit model of the induction cooker.

Finally, the capacitance of the resonant capacitor is selected to model the HBSRC for IH. The IH characteristics, such as high quality factor Q and high slope of the resonant current versus frequency, of the copper pan obtained through quantitative prediction can be used to develop control methodologies.

A. COILS AND LITZ WIRE SELECTIONS

The IH specifications are presented in Table 2. Fig. 4 displays the equivalent circuit model of the induction cooker with the pan. The other design baselines of the induction coil are as follows:

- (i) The gap between the coil and pan is 2 mm.
- (ii) The copper pan is located at the center of the induction coil.
- (iii) The coil comprised an equivalent #6 AWG (4 mm) 3200-strand #AWG 44 Litz wire to reduce the skin effect. The resistance per unit length of the stranded Litz wire is measured using the impedance analyzer because the Litz wire is too complex for simulating the resistance using Maxwell 3D [26], [27].
- (iv) The simulation temperature of environment is set as 25 °C.

To conduct accurate simulation of the pan resistance, the thickness of each layer of the bottom side of the pan was set as 0.073 mm, which is less than half of the skin depth of copper at 200 kHz. The other simulated parameters are presented in Table 3. Fig. 4 displays the equivalent circuit model of the induction cooker. If the resonant circuit loss is

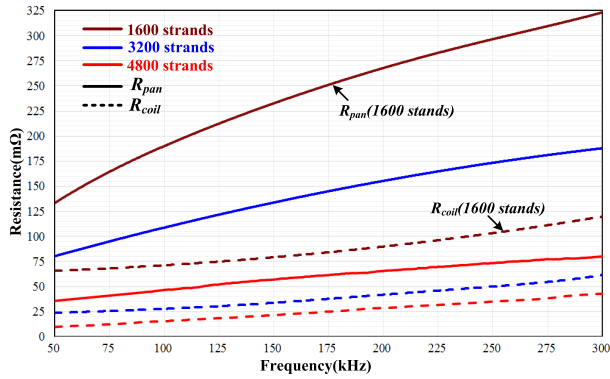


FIGURE 5. Measured R_{coil} and R_{pan} of various Litz wires under the same coil diameter (200 mm) with the same copper pan.

neglected, the heating efficiency can be expressed as follows:

$$\eta = \frac{P_{pan}}{P_{pan} + P_{loss}} = \frac{R_{pan}}{R_{eq} + R_{circuit}} \approx \frac{R_{pan}}{R_{eq}} \quad (1)$$

where

R_{pan} : equivalent resistance of the pan.

R_{coil} : equivalent resistance of the coil.

$P_{loss} (= P_{circuit} + P_{coil})$: power loss of the resonant circuit.

$R_{eq} = R_{pan} + R_{coil}$: equivalent resistance of induction coil with a pan.

$R_{circuit} (\ll R_{eq})$: resonant circuit resistance, which includes the ESR of the resonant capacitor and current sensor as well as the power trace of the printed circuit board (PCB).

1) LITZ WIRE SELECTION

Because R_{pan} and R_{coil} are the key factors influencing the heating efficiency, the R_{pan} and R_{coil} values for the 15-turn and 4800-strand #AWG 44 Litz wire are compared with those for the 21-turn and 3200-strand #AWG 44 Litz wire and the 29-turn and 1600-strand #AWG 44 Litz wire shown in Fig. 5 under the same coil diameter with the same copper pan shown in Table 1. Fig. 6 and Table 3 present a comparison of the parameters and efficiency of the aforementioned three Litz wire coils obtained using (1). R_{pan} is proportional to the square-root of frequency due to the skin effect, but the R_{coil} is nonlinear function of frequency because of the proximity-effect on Litz wires [28]. Although Table 3 indicates that the 15-turn Litz wire has the lowest R_{coil} , the R_{pan} of the 21-turn Litz wire is larger than that of the 15-turn wire. Therefore, the heating efficiency of the 21-turn Litz wire is 4.3% higher than that of the 15-turn Litz wire. Consequently, the 21-turn induction coil is selected for the developed IH system.

2) INFLUENCE OF THE COIL TURN ON HEATING POWER AND THE HEATING EFFICIENCY

Fig. 7 illustrates the measured resistance of the Litz wire spiral coils for various turns. The results indicate that the resistance of the spiral coil is proportional to the length of coil at various frequencies. Therefore, these results can be used to estimate the resistance of the Litz coil. The aforementioned

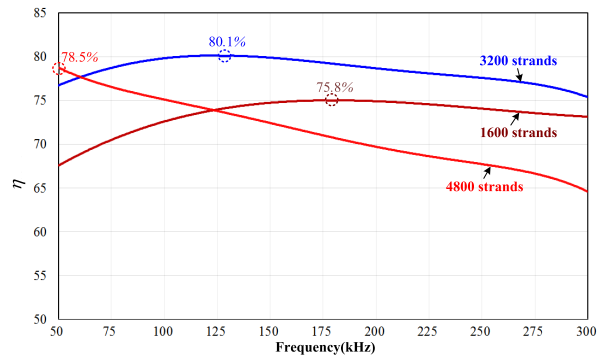





FIGURE 6. Comparison of the heating efficiencies of various Litz wires under the same coil diameter (200 mm).

TABLE 3. Key parameters of the copper pan.

Coil diameter	200 mm		
Copper pan diameter(bottom)	155 mm		
Gap between pan and winding	2 mm		
Operating frequency	100 kHz		
Strands of Litz wire	4800	3200	1600
Coil turns	15	21	29
Coil shape			
L_{eq} (measured/FEA*)	7.2 μH/ 7.1 μH	9.9 μH /10.5 μH	17.4 μH /18.3 μH
R_{pan} (measured/FEA)	47 mΩ/ 52 mΩ	112 mΩ /109 mΩ	193 mΩ /188 mΩ
R_{coil} (measured)	15.5 mΩ	28 mΩ	72 mΩ
$R_{eq} = R_{coil} + R_{pan}$ (measured)	62.5 mΩ	140 mΩ	265 mΩ
$\eta (\approx \frac{R_{pan}}{R_{eq}})$	75.2%	80.0%	72.8%

*FEA: simulated value obtained using Maxwell 3D.

approach can replace complex and time-consuming software simulation for the calculation of the Litz wire resistance. The following results are obtained from the simulations of the pan power and efficiency for various turns of the 3200-strand Litz wire shown in Fig. 8:

- (i) The pan power is highly proportional to the number of coil turns at various frequencies. Although an increase in the number of turns can increase the output power, the size limitation of the coil diameter should be considered.
- (ii) Due to the higher resistance of the induction coil in higher operating frequency, the heating efficiency and power at 100 kHz operating frequency will be higher than 200 kHz.

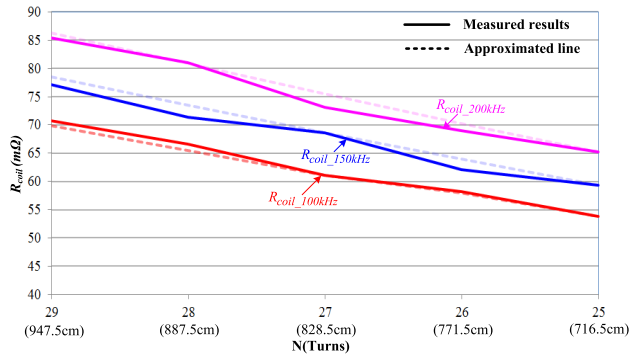


FIGURE 7. Measured results of the coil resistance of the spiral Litz wire versus the coil length.

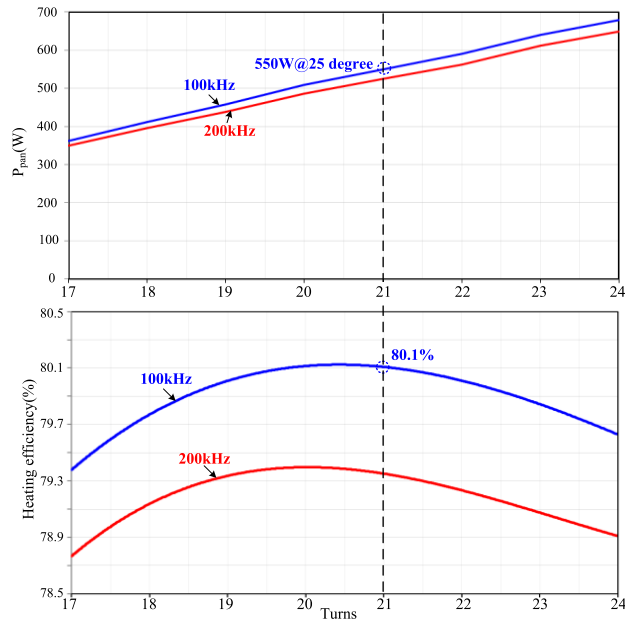


FIGURE 8. Simulated results for the induction coil made of the 3200-strand Litz wire.

- (iii) The maximal efficiency is 80.1% for 21 turns at 100 kHz (same value as in Table 3).

B. CHARACTERISTICS OF THE HBSRC FOR THE COPPER PAN

1) INDUCTANCE ANALYSIS WITH AND WITHOUT THE COPPER PAN

According to the design process, the 21-turn and 3200-strand Litz wire is used as the induction coil. The coil inductance without and with the copper pan can be expressed as follows:

$$L_{coil} = \frac{\phi_{coil}}{i_{re}} = \frac{N_e^2}{\mathfrak{R}} \quad (2)$$

$$L_{eq} = \frac{\phi_{coil} - \phi_{eddy}}{i_{re}} \quad (3)$$

where

L_{coil} and L_{eq} : coil inductance without and with the copper pan, respectively.

ϕ_{coil} : total flux generated by the coil without the pan.

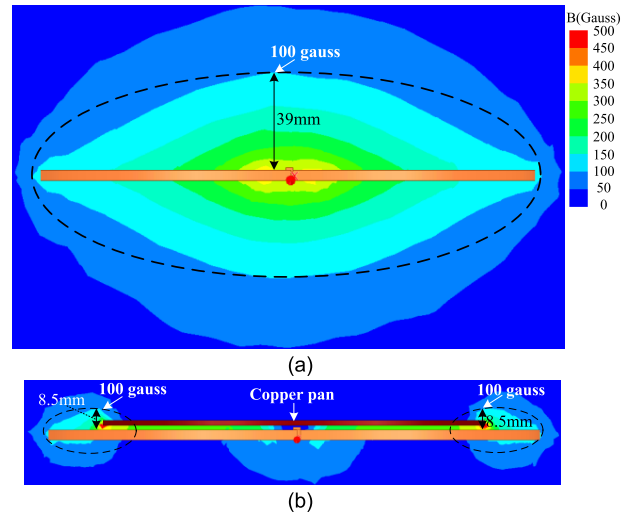


FIGURE 9. Flux density distribution and L_{eq} obtained through Maxwell 3D: (a) without the copper pan; (b) with the copper pan; (c) L_{eq} .

ϕ_{eddy} : total flux generated by the eddy current on the bottom of the pan.

N_e : equivalent turns of the coil.

\mathfrak{R} : MAGNETIC RESISTANCE.

The equivalent inductance with the copper pan L_{eq} is smaller than the coil inductance L_{coil} without a pan by (2) and (3), because of the negative flux of eddy current. The field simulation software Maxwell 3D is used to simulate L_{eq} and the magnetic flux distribution with and without the copper pan on the induction coil is shown in Fig. 9. The simulation results are briefly described as follows:

- (i) The magnetic flux generated by the induction coil without the pan is naturally and symmetrically distributed on both sides of the coil, as displayed in Fig. 9(a). However, when the copper pan is placed on the coil, the magnetic flux decreased and most of the magnetic flux is concentrated between the coil and the bottom of the copper pan, as displayed in Fig. 9(b). This phenomenon occurred mainly due to the eddy current generated by the penetration of the magnetic flux into the pan bottom.
- (ii) The L_{eq} values displayed in Fig. 9(c) are $10.5\mu H$ and with and $36.4\mu H (= L_{coil})$ without the copper pan on the coil, respectively.

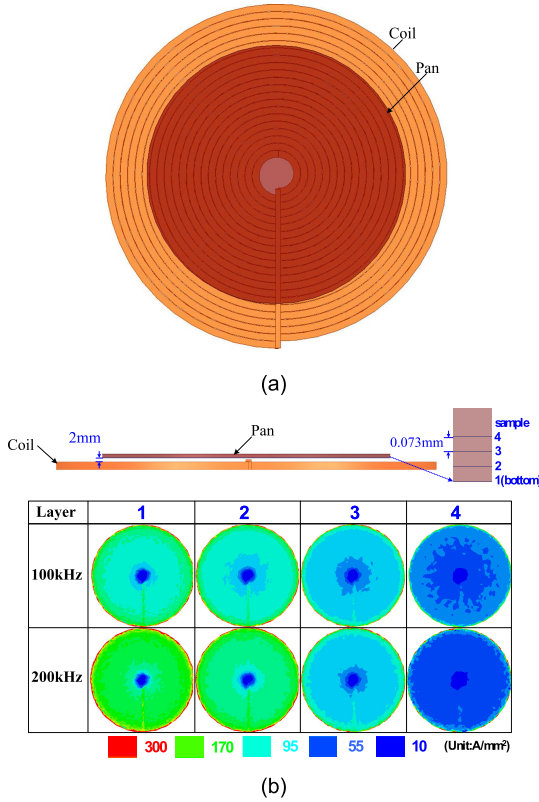


FIGURE 10. Eddy current density distribution at the bottom of the copper pan with 55 Arms and 21 turns at 100 kHz and 200 kHz: (a) top view of the induction coil; (b) various samples of the skin depth.

2) OPERATION FREQUENCY DESIGN

Fig. 10 illustrates the eddy current density distribution generated at the bottom side of the copper pan by the 100 kHz and 200 kHz resonant currents. The simulation results revealed that the eddy current density is more concentrated on the surface or sample 1 of the pan. The AC resistance of the pan increased with an increase in the frequency.

$$R_{ac} = \frac{l}{\rho A_{eff}} \approx \frac{l\rho}{\pi D\delta}, \text{ if } D \gg \delta \quad (4)$$

where

$\delta (= \sqrt{\frac{\rho}{\pi f \mu}})$: penetration depth of the flux.

μ : permeability.

ρ : conductivity.

D : thickness of bottom of the copper pan.

Fig. 11 illustrates the influence of the operating frequency on the heating efficiency, R_{pan} , and R_{coil} of the 21-turn and 3200-strand Litz wire. In this study,

- (i) R_{pan} is simulated using Maxwell 3D and increased with an increase in the frequency;
- (ii) R_{coil} is calculated using the method displayed in Fig. 7;
- (iii) the heating efficiency η decreased due to the higher increase in R_{coil} than in R_{pan} under increasing frequency. The maximal heating efficiency is 80% at 130 kHz. Therefore, the resonant frequency is selected near 130 kHz.

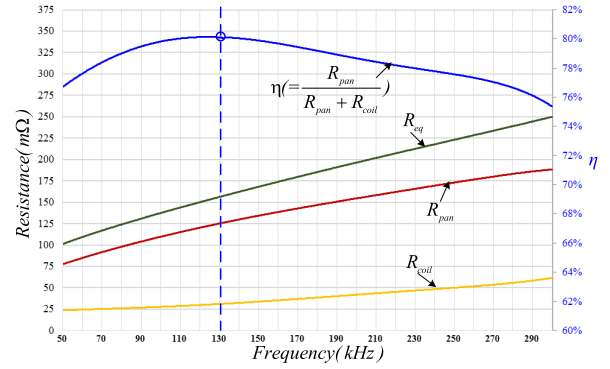


FIGURE 11. R_{pan} , R_{coil} , and η versus the frequency for the 21-turn and 3200-strand Litz wire.

C. RESONANT CAPACITOR AND CURRENT

1) RESONANT CAPACITANCE

According to the specifications in Table 2, the induction coil made of a 21-turn and 3200-strand Litz wire exhibits its maximum efficiency at 130 kHz. The required resonant capacitance is calculated to be 142.7 nF when $L_{eq} = 10.5 \mu H$.

2) RESONANT CURRENT

The characteristics of the resonant current are key factors for calculating the heating power, performing pan detection, and developing control algorithms for the copper pan. For the HBSRC converter displayed in Fig. 2, the peak resonant current can be derived using the following expression:

$$I_{rep} = \left| \frac{v_{Req}(s)}{R_{eq}} \right| = \frac{2V_{dc}}{\pi |Z_{re}|} = \frac{2V_{dc}}{\pi \sqrt{R_{eq}^2 + (\omega L_{eq} - \frac{1}{\omega C_r})^2}} = \frac{2V_{dc}}{\pi \sqrt{1 + Q^2 (\frac{f_r}{f_s} - \frac{f_s}{f_r})^2}} \quad (5)$$

where

$|v_{Req}(s)| (= \frac{2V_{dc}}{\pi} \frac{R_{eq}}{|Z_{re}|})$: voltage amplitude of the R_{eq} derived using the first-harmonic method.

$$Z_{re} = R_{re} + j(X_{L_r} - X_{C_r})$$

$$R_{re} = R_{pan} + R_{coil} + R_{circuit}$$

$$Q = \frac{1}{R_{eq}} \sqrt{\frac{L_{eq}}{C_r}} \text{ (if one neglects the } R_{circuit} \text{ due to } R_{circuit} \ll R_{eq})$$

The simulated RMS resonant current $i_{rs,rms}$ for various R_{eq} values is displayed in Fig. 12. The following conclusions were obtained:

- (i) The parameter $i_{rs,rms}$ increased rapidly when the operating frequency is close to the resonant frequency because the R_{eq} value of the copper pan is smaller than that of the ferromagnetic pan.
- (ii) To reduce the switching loss of the MOSFET in the half-bridge, the operating frequency is set to be higher than f_r for reaching the ZVS.
- (iii) The derivative of i_{re} by frequency, $\frac{d}{df} i_{re,rms}$, at the operating frequency 135 kHz is 40A_{rms}/kHz. Thus, the HBSRC

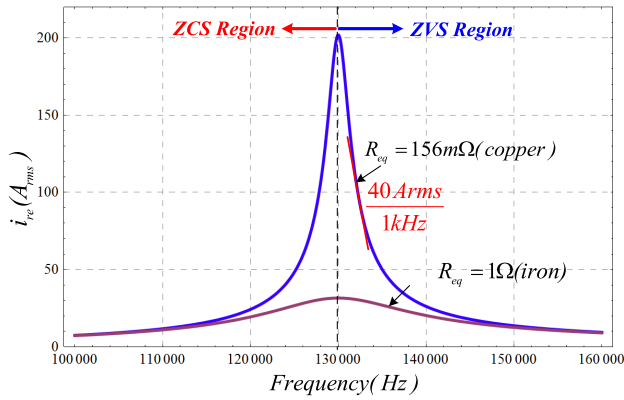


FIGURE 12. Simulated $i_{re,rms}$ values versus operating frequency of the proposed IH system.

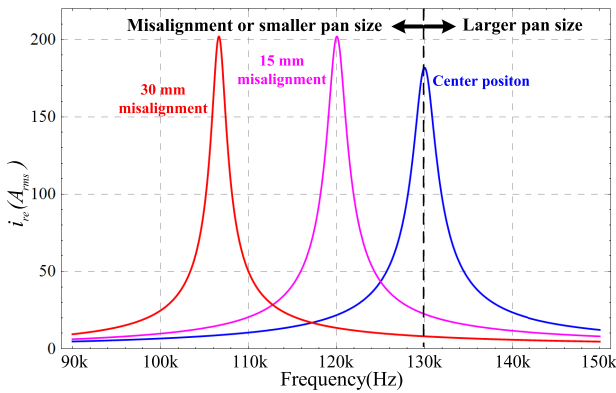


FIGURE 13. Resonant current curve for various pan conditions.

should provide a high-resolution operating frequency to reduce low-frequency oscillations for heating power control.

D. RESONANT FREQUENCY ESTIMATION

The high Q factor of the copper pan, misalignment of the pan position, and variation of the copper pan size caused variations in the operation frequency shown in Fig. 13. The proposed function for the estimation of the resonant frequency is used to determine the optimal operation frequency range. Because of the low resistance of the copper pan, the impedance of the resonant tank (Z_{re}) can be simplified as follows when the operating frequency is higher than the resonant frequency shown in Fig. 14:

$$Z_{re} \approx j(X_{Lr} - X_{Cr}) \quad (6)$$

Assume the resonant current $i_{re}(t)$ is dominated by the fundamental component $i_{re1}(t)$, the following expression is obtained:

$$i_{re}(t) \approx i_{re1}(t) = I_{rep} \sin(\omega_s t + \theta) \quad (7)$$

Therefore, the estimated inductance $L_{r,est}$ and resonant frequency $\omega_{r,est}$ are expressed as follows:

$$L_{r,est} \approx \frac{1}{2\pi f_s} \left(K + \frac{1}{2\pi f_s C_r} \right) \quad (8)$$

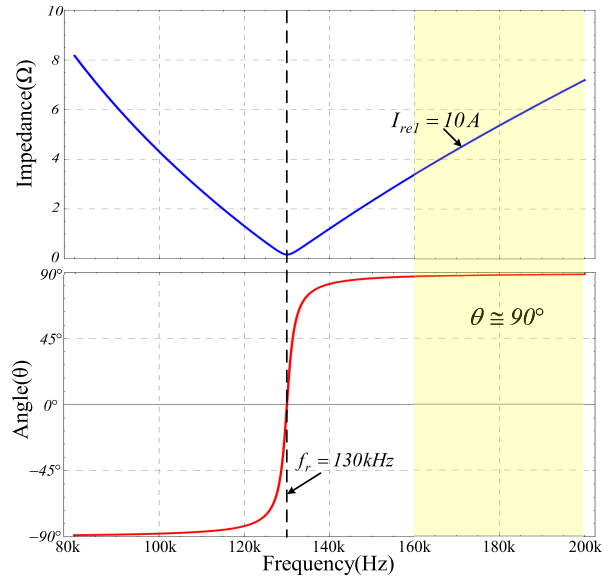


FIGURE 14. Simulated results for the resonant tank impedance and angle.

$$f_{r,est} = \frac{1}{2\pi \sqrt{L_{r,est} C_r}} = f_s \sqrt{\frac{1}{2\pi f_s K C_r + 1}} \quad (9)$$

where

$$K = \frac{v_{dc} \times \frac{2}{\pi}}{I_{rep}}$$

According to (8) and (9), the estimated resonant frequency $f_{r,est}$ can be calculated using the given operating frequency, known resonant capacitance, and given amplitude of the resonant current.

E. BUCK CONVERTER

The proposed specifications of the buck converter are presented in Table 1. The DC link voltage is controlled from 35 V to 70 V to satisfy various heating power demands. Moreover, a SiC MOSFET and synchronous control are adopted on Q1 and Q2 to achieve high efficiency. The key component selection are described in the following text:

1) INDUCTANCE

The inductor current ripple is designed to be 25% of the peak DC link current. The calculated inductor current ripple was 100 μ H, and TDK ferrite core ETD 59 is used to construct the inductor.

2) DC LINK CAPACITORS

To achieve passive power factor correction, and proposed DC link voltage control method, the small capacitance is designed to be 33 μ F and a low-ESR film capacitor with high RMS current capacity is selected.

III. CONTROL METHODOLOGIES

Fig. 2 illustrates the established IH converter with the proposed control schemes, which consist of the resonant

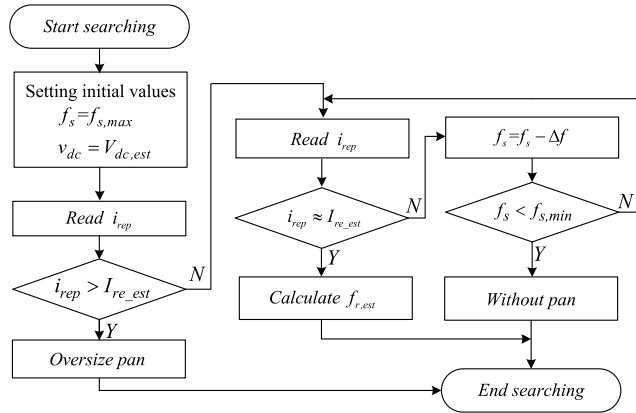


FIGURE 15. Flowchart of the process for searching the resonant frequency.

frequency estimator for initialization to determine the operating frequency, and heating power control for cooking. The proposed schemes are described in the following text.

A. RESONANT FREQUENCY ESTIMATION

It is used to estimate the resonant frequency of pans of various sizes or to detect misalignment. According to (9), $f_{r,est}$ can be expressed as follows:

$$f_{r,est} = f_s \sqrt{\frac{1}{1 + (\frac{4v_{dc}}{I_{rep}} C_r) f_s}} \tag{10}$$

For a given C_r, f_s , sensing peak value of the resonant current I_{rep} , and DC link voltage v_{dc} , the on-line calculation of $f_{r,est}$ by using a look-up table is convenient. The flowchart of the process for searching the resonant frequency is displayed in Fig. 15. First, the initial values and searching resonant frequency are set according to I_{rep} . If the size of the pan is larger than maximal size, I_{rep} is larger than $I_{re,est}$ at the initial frequency $f_{s,max}$, and the system ends frequency searching. When I_{rep} reaches the default value $I_{re,est}$, the estimated resonant frequency $f_{r,est}$ can be obtained using (10). The maximal and minimal operating frequencies $f_{s,max}$ and $f_{s,min}$ can be determined from the simulated results obtained using Maxwell 3D and MATLAB. The maximal and minimal frequencies are dependent on the maximal pan size and without pan on the induction coil, respectively.

B. HEATING POWER CONTROL WITH PFC

To control the heating power and satisfy harmonics requirements simultaneously, the proposed control schemes are used shown in Fig. 16. These schemes are described in the following text.

1) POWER CONTROL OF THE COPPER PAN

To achieve power control, a simple heating power estimator is developed. The estimated heating power of pan P_{pan} can be

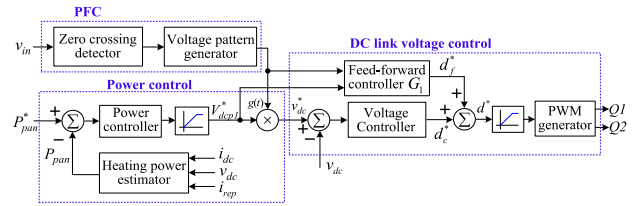


FIGURE 16. Functional block of the heating power control with the PFC.

expressed as follows:

$$P_{pan} = \eta_{HB} v_{dc} i_{dc} - \frac{1}{2} i_{rep}^2 (R_{coil} + R_{misc}) \tag{11}$$

where

η_{HB} : efficiency of the HBSRC caused by switching and conduction loss.

i_{rep} : peak current of i_{re} .

R_{misc} : miscellaneous resistance in the resonant tank, which consists of a current sensor, main power path of the PCB, and ESR of the resonant capacitor.

The power controller is constructed using a PI-type regulator, which generates a peak fundamental voltage command V_{dcp1}^* to reach the required DC link voltage for the HBSRC. Due to the MOSFETs operating in the ZVS region, the switching losses of the HBSRC and η_{HB} can be expressed as follows:

$$P_{loss_sw} \approx 2E_{off} f_s \tag{12}$$

$$P_{loss_cond} \approx \frac{I_{rep}^2 \times R_{dson}}{2} \tag{13}$$

$$\eta_{HB} = \frac{v_{dc} i_{dc} - P_{loss_cond} - P_{loss_sw}}{v_{dc} i_{dc}} = 1 - \frac{2E_{off} f_s}{i_{dc}} - \frac{I_{rep}^2 R_{dson}}{2} \tag{14}$$

2) THIRD-HARMONIC INJECTION OF THE DC LINK VOLTAGE COMMAND

To satisfy the IEC-61000-3-2 standard, a voltage pattern generator with third-harmonic injection was used to produce the waveform $g(t)$ of the DC link voltage command v_{dc}^* . The maximal permissible third-harmonic current should be less than $2.3A_{rms}$ according to IEC-61000-3-2-2014 Class A for household appliances. Therefore, the proposed v_{dc}^* is expressed as follows:

$$v_{dc}^* = V_{dcp1}^* g(t) \tag{15}$$

where

K_v : ratio of third DC link voltage harmonic

$$g(t) = |(\sin \omega_1 t + K_v \sin 3\omega_1 t)|$$

If the line voltage v_{ac} is sinusoidal and f_s is fixed, then the DC link power p_{dc} is expressed as follows:

$$p_{dc} = \frac{v_{dc}^2}{Z_{SRC}} = \eta_{buck} v_{ac} i_{ac} \tag{16}$$

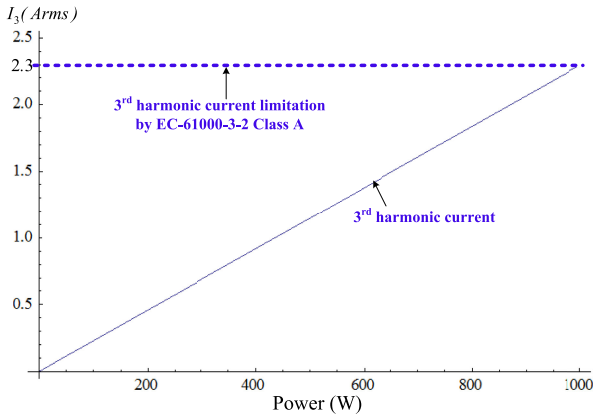


FIGURE 17. Simulated results for the third-harmonic current under various loads under the of the rated load.

where

Z_{SRC} : equivalent input impedance of the HBSRC under a fixed operating frequency.

η_{buck} : efficiency of the buck converter.

$v_{ac}(t) [= V_p \sin \omega_1 t]$: line voltage.

Let $i_{ac}(t) = I_1 \sin \omega_1 t + I_3 \sin 3\omega_1 t$ By substituting (15) into (16), the following expression is obtained:

$$I_1 = \frac{V_{dcp1}^2}{Z_{SRC}(\eta_{buck} V_p)} \quad (17)$$

$$I_3 = 2K_V I_1 \quad (18)$$

where K_V can be calculated according to (18) under the following conditions:

- (i) $I_3 = 2.3\sqrt{2}$ given by the IEC-61000-3-2-2014 Class A standard.
- (ii) Maximum power of 1000 W.
- (iii) Line voltage of 110 V.
- (iv) $\eta_{buck} = 0.95$.

We obtained the following values: $K_V = 0.12$ and $PF = 0.97$.

To maintain the same power factor for various heating power conditions, we fix K_V as 0.12 in the proposed control loop. Fig. 17 displays the simulated result for the third-harmonic current under various loads. The aforementioned figure indicates that the K_V value enabled the third-harmonic current to satisfy the IEC-61000-3-2-2014 Class A standard.

3) DC LINK VOLTAGE CONTROL

If excellent DC link voltage control is achieved using (15), the heating power of the pan P_{pan} can be expressed as follows:

$$P_{pan} = V_{dcp1}^* 2 \left[\frac{2(1 + K_V^2)}{\pi} \right] \times \frac{R_{pan}}{|Z_{re}| R_{eq}} \quad (19)$$

where

$$|Z_{re}| = \sqrt{R_{re}^2 + (X_{Lr} - X_{Cr})^2}$$

$$R_{re} = R_{pan} + R_{coil} + R_{circuit}$$

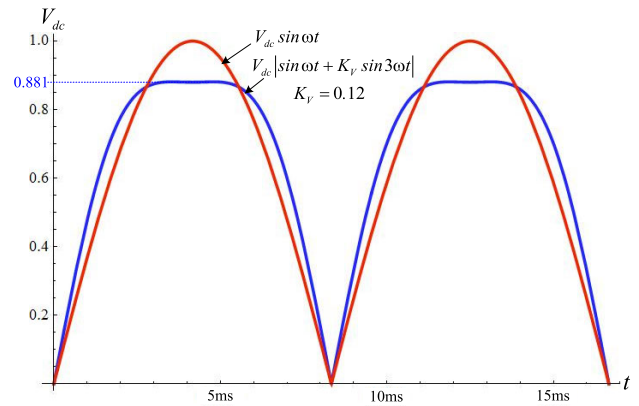


FIGURE 18. Voltage command waveform with the proposed method ($K_V = 0.12$).

Thus, P_{pan} can be controlled by V_{dcp1}^* and K_V under a fixed operating frequency to replace the traditional variable frequency method, as displayed in Fig. 16. Consequently, the low-frequency oscillations caused by inaccurate operating frequencies are reduced. Moreover, the PI voltage controller and a voltage feedforward controller G_1 are adopted to obtain excellent voltage command tracking. On the basis of (15), G_1 can be derived by voltage gain of buck converter expressed as follows:

$$G_1(t) = \frac{V_{dcp}^*}{v_{in}} (1 + K_V \frac{|\sin 3\omega t|}{|\sin \omega t|}) \quad (20)$$

4) COMPARISON OF THE POWER CONTROL METHODS

The peak voltage of the proposed method determined from the differential of (15), which yields $V_{dc,peak} = 0.881 V_{dcp1}$ at $3.54ms$ when $K_V = 0.12$. Therefore, the peak current of the proposed method was 0.881 times the $I_{re,peak}$ of the traditional method ($K_V = 0$). The power expansion ratio between the proposed and traditional method derived from (19) under the same $V_{dc,peak}$ and $I_{re,peak}$ is expressed as follows:

$$\frac{P_{pan}(proposed K_V = 0.12)}{P_{pan}(traditional)} = \frac{(1 + K_V^2)}{0.881^2} \quad (21)$$

Fig. 18 displays the simulated DC link voltage of the proposed method. For the same limitations of $I_{re,peak} = 100A$, and $V_{dcp} = 70V$, the simulation results presented in Table 4 and Fig. 19 indicates the proposed control method can provide 31% higher power than the traditional control method.

IV. EXPERIMENTAL RESULTS

Fig. 20 displays the experimental setup for the proposed IH system. The setup consists of a front-end buck converter with an AC-DC rectifier, an HBSRC, a DSP (TMS320F28075)-based controller, and an induction coil with the copper pan. The tested conditions and functional block of the proposed controller are presented in Table 2.

TABLE 4. Comparison of the dc link input power of various control methods according to PSIM.

	Traditional method	Proposed method
Resonant current Limitation(peak)	100A	
DC-link voltage	$V_{dc, peak} = 70\text{ V}$	
Switching frequency	132 kHz	
Simulated results	490W	645W
Power output(p.u.)	1	1.32 (design value 1.31)

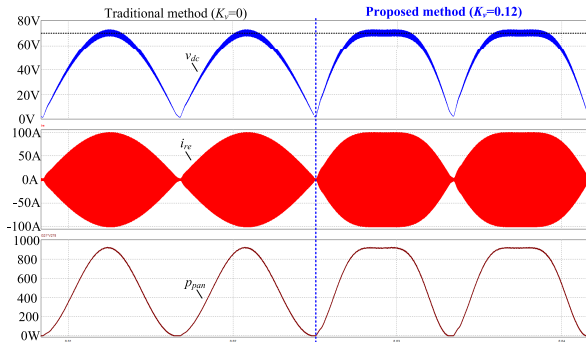


FIGURE 19. Simulation results of the DC link input power for the traditional and proposed methods.

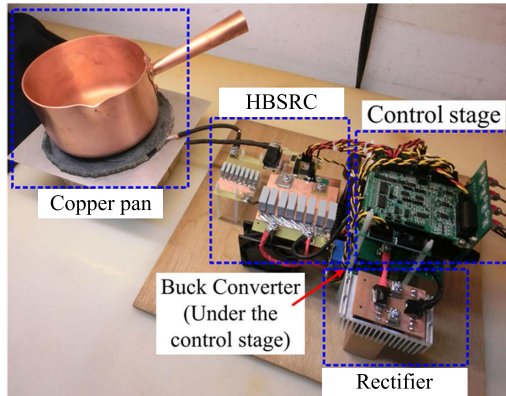


FIGURE 20. Experimental setup of the proposed IH system.

A. COIL CONSTRUCTION AND PARAMETER MEASUREMENT

The coil winding is selected according to the results of the aforementioned analysis. The selected coil winding is a 21-turn, 0.05-mm, and 3200-strand Litz wire with a diameter of approximately 200 mm. Moreover, the thermoset plastics Epoxy is used to fix coils and assist heat dissipation. The procedure of constructing the coil winding and measurement setup are displayed in Fig. 21.

Fig. 22 displays the simulated and measured parameters of the proposed IH system with copper pan. Because no magnetic saturation occurred, we use an impedance analyzer (WK 6500B) to measure the equivalent parameters of IH with the copper pan. The results reveal that the maximal difference between measurement and simulation is less than 7%.

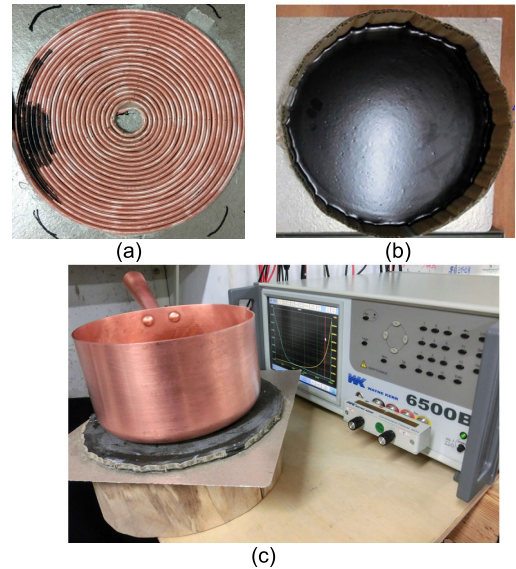


FIGURE 21. Coil winding and measurement setup: (a) induction coil; (b) Induction coil with epoxy; (c) parameter measurement setup with impedance analyzer.

B. COIL CONSTRUCTION AND PARAMETER MEASUREMENT

1) BUCK CONVERTER

Fig. 23 illustrates the measured efficiency of the buck converter at various output voltages. The output power is proportional to the output voltage v_{dc} , and the equivalent impedance of IH with the copper pan is lower than that with the ferro-magnetic pan. The rated power is set as 1 kW at a 70-V output voltage. The efficiency of the proposed approach is more than 97.5% when the output power is larger than 18% of the rated power.

2) HBSRC WITH THE COPPER PAN

(i) ZVS turn-on operation

Since ZVS operation is very important to reduce the switching loss of the HBSRC. Fig.24 shows that the proposed HBSRC provides ZVS turn-on under different loaded conditions.

(ii) Efficiency measurement

To obtain accurate efficiency measurements, the tested copper pan is filled with 1.5 L of water, is displayed in Fig. 25(a). The copper pan is wrapped with Styrofoam for thermal insulation as displayed in Fig. 25(b). The ambient temperature is 25°C. The average power is measured using a digital scope (RTO 1014) with 16-bit vertical resolution in the high-definition mode. The average output power and efficiency of the copper pan can be expressed as follows:

$$P_o = P_{re} - P_{circuit} - P_{coil} = i_{re,rms}^2 R_{pan} \quad (22)$$

$$\eta = \frac{P_o}{P_{dc}} \quad (23)$$

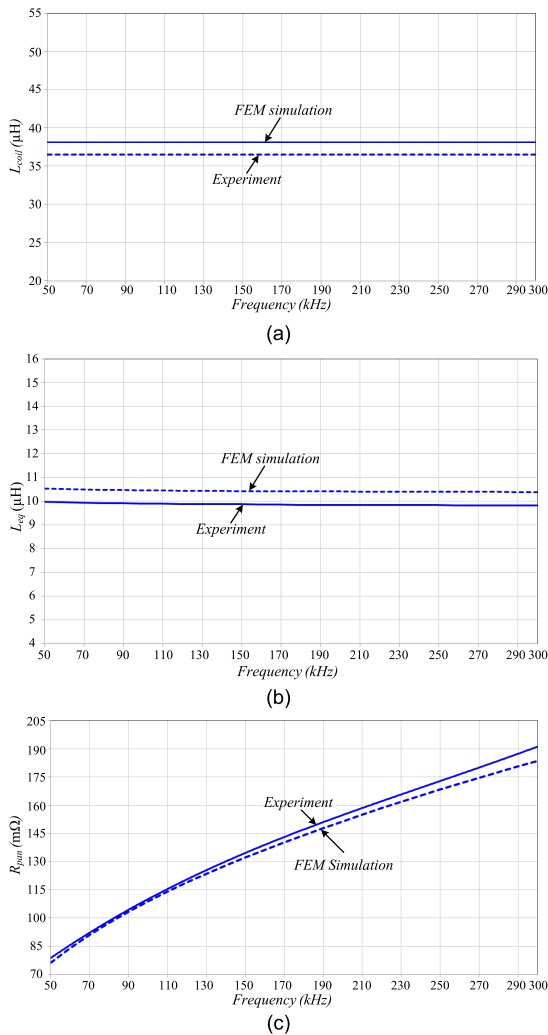


FIGURE 22. Experimental setup of the proposed IH system: (a) coil inductance without the pan; (b) coil inductance with the pan; (c) equivalent pan resistance R_{pan} .

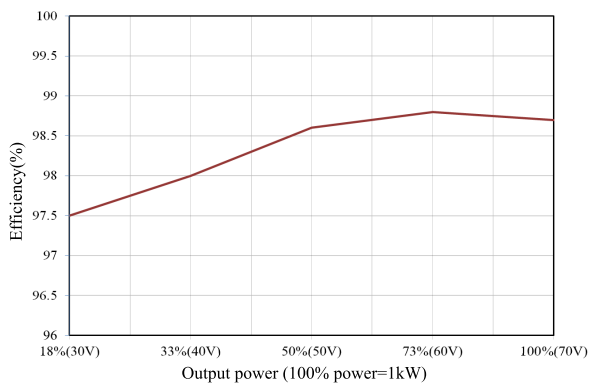


FIGURE 23. Efficiency measurement under various power and v_{dc} conditions.

where

$$P_{dc} = \frac{\int_0^{T_{total}} v_{dc}(t) \times i_{dc}(t) dt}{T_{total}}$$

$$P_{re} = \frac{\int_0^{T_{total}} v_{re}(t) \times i_{re}(t) dt}{T_{total}}$$

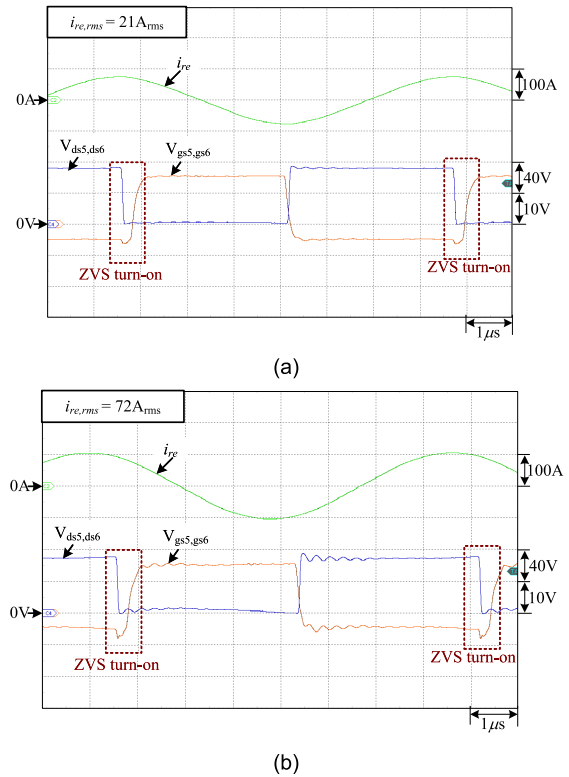


FIGURE 24. ZVS operation in different heating power conditions: (a) $P_{pan} = 55W$; (b) $P_{pan} = 648W$.

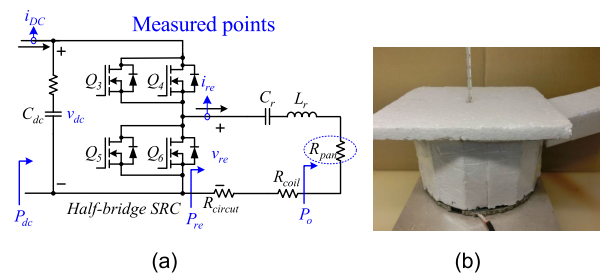


FIGURE 25. Test platform of the proposed IH system with the copper pan: (a) $P_{pan} = 55W$; (b) Induction coil and a copper pan with Styrofoam.

$$P_{circuit} = i_{re,rms}^2 \times R_{circuit}$$

$$P_{coil} = i_{re,rms}^2 \times R_{coil}$$

Because copper is a temperature-dependent material, the coil resistance and pan resistance at a fixed operation frequency can be expressed as follows:

$$R_{coil} = R_{coil}(25^\circ C) \times \frac{(234.5 + T)}{(234.5 + 25)} \quad (24)$$

$$R_{pan} = R_{pan}(25^\circ C) \times \frac{(234.5 + T)}{(234.5 + 25)} \quad (25)$$

Fig. 26, Fig. 27 and Table 5 present the measured results of the resonant tank, the power loss distribution, and the measured power and efficiency of the proposed IH system with the copper pan, respectively. The following conclusions are obtained from the measured results:

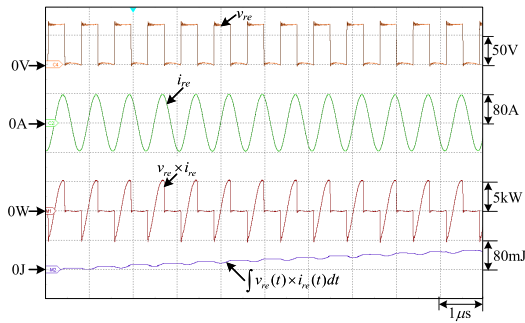


FIGURE 26. Measured and calculated results of resonant tank using the digital scope (R&S RTO 1014).

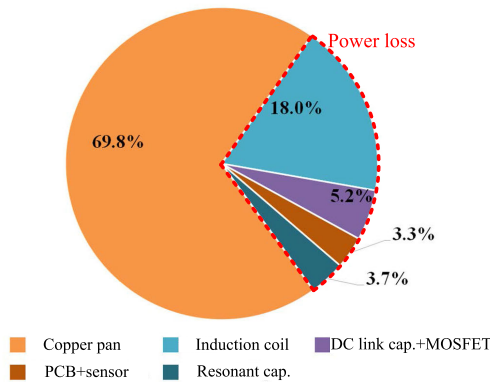


FIGURE 27. Power distribution of the proposed HBSRC with the copper pan ($P_{dc} = 612$ W and 132 kHz).

TABLE 5. Measured power and efficiency of the proposed IH with copper pan ($f_s = 132$ kHz).

i_{re}	52.4Arms	T_{water}	93°C
PCB + sensor loss	20.4W	P_{cr}	22.6W (8.25mΩ)
$P_{mos}(P_{dc} - P_{re})$	32W	P_{re}	580W
$P_{coil}(93°C)$	110W	P_{dc}	612W
P_o	427W(155.8mΩ)	Coil efficiency	79.5%
	(WK measured 165mΩ)		$P_o / (P_o + P_{coil})$
Total Efficiency P_o / P_{dc}			69.8%

- (i) The total efficiency of the HRSRC with the copper pan is 69.8% at 93 °C.
- (ii) Due to the low heating resistance of the copper pan, copper losses from the coil accounted for 60% of the total losses.
- (iii) The measured coil efficiency [$P_o / (P_o + P_{coil})$] is 79.5%, which is consistent the results of the proposed calculation method (Fig. 11).

C. VERIFICATION OF THE CONTROL METHODOLOGIES

1) RESONANT FREQUENCY ESTIMATION

The proposed resonant frequency estimation method is verified for various conditions of misalignment of the copper

TABLE 6. Resonant frequency estimation ($v_{dc} = 70V, I_{rep} = 10A$).

Pan position	Measured results (Impedance analyzer)		Estimation results		Error (%)
	$L_r(\mu H)$	$f_r(kHz)$	$L_r(\mu H)$	$f_r(kHz)$	
Center	9.9	130	9.5	134	3.0
Shift 1.5cm	11.6	121	11.2	123	1.8
Shift 3cm	14.7	108	14.2	109	1.0

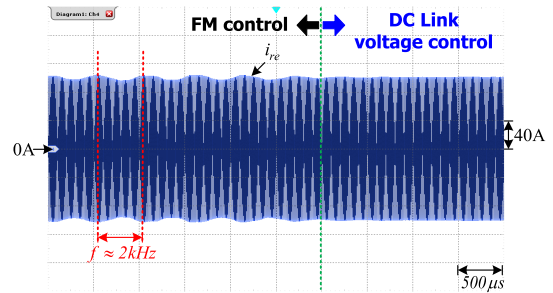


FIGURE 28. Comparison of the resonant current measurements obtained with the FM control and a fixed-frequency DC link voltage control methods.

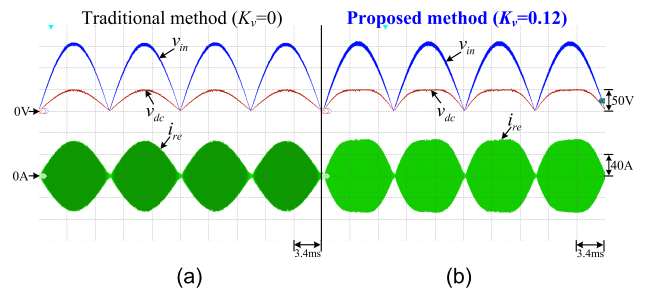


FIGURE 29. Experimental results of the DC link voltage control method ($V_{ac,rms} = 110$ V, $f_s = 132$ kHz, $V_{dc,peak} = 50$ V, and $I_{re,peak} = 70$ A): (a) traditional ($P_{dc} = 245W$); (b) proposed ($P_{dc} = 324W$).

pan on the coil. The experimental results obtained using the impedance analyzer and the estimation results are presented in Table 6. The maximum error of the proposed estimation method was less than 3%.

2) POWER CONTROL USING THE DC LINK VOLTAGE WITH THIRD-HARMONIC INJECTION

The proposed DC link voltage control method with a fixed switching frequency exhibits a stable performance and without low frequency peak current ripple on the resonant current compared to traditional frequency modulation (FM) method as shown in Fig. 28. Wherein, the traditional FM method exists 2 kHz peak current ripple which may induce acoustic noise.

The proposed power control method by controlling the DC link voltage v_{dc} is verified and compared to traditional control method shown in Fig.29 and Fig.30. The proposed method can reach input power P_{ac} of 494 W and 650 W under $V_{dc,peak} = 50V, I_{re,peak} = 70$ A and $V_{dc,peak} = 50V, I_{re,peak} = 100$ A, respectively. All of the power are near 32%

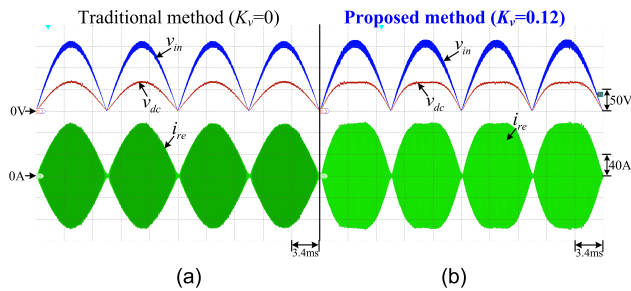


FIGURE 30. Experimental results of the DC link voltage control method ($V_{ac,rms} = 110$ V, $f_s = 132$ kHz, $V_{dc,peak} = 70$ V, and $I_{re,peak} = 100$ A): (a) traditional ($P_{dc} = 494$ W); (b) proposed ($P_{ac} = 650$ W).

TABLE 7. Experimental results of different control methods.

	Traditional method	Proposed method
$I_{re,peak}$	100 A	
$V_{dc,peak}$	70 V	
Simulated results	494W	650W
Power output(p.u.)	1	1.32 (design 1.31)

higher than the traditional method at the same operating conditions, which are match to the analyzed results. Moreover, the power factor is 0.96 at 650W output power which is closed to the designed value (0.97) shown as Table 7.

V. CONCLUSION

This paper presents a Maxwell-3D-assisted IH design process for copper pans to achieve optimal efficiency. A DSP-based digitally controlled IH system for copper pan, which includes an AC-DC rectifier, a buck converter, and a HBSRC with an optimal design induction coil, is implemented to verify the proposed design process and control methods. Analysis and Maxwell 3D simulation are verified using the measured results. The key contributions of this paper can be summarized as follows:

1) The proposed IH design process involves the selection of Litz wire, determination of the optimal number of coil turns, and design of the resonant frequency to achieve the optimal efficiency by using the Maxwell-3D and the per unit coil resistance R_{coil} . Finally, a 21-turn and 3200-strand #AWG 44 IH coil is selected, and the resonant frequency of the HBSRC is 130 kHz; thus, a coil efficiency of 80% is achieved. The performance of the selected coil is verified by obtaining experimental results.

2) The Maxwell 3D simulated results of the equivalent coil parameters L_{coil} , L_{eq} , and R_{pan} are verified using an impedance analyzer, and the error between the simulated and experimental results is less than 6%.

3) A resonant frequency estimation method is proposed to provide a suitable operation frequency under non-ideal conditions, such as misalignment of the pan position and varying pan size.

4) A power control method involving DC link voltage control with third-harmonic injection is proposed to provide a stable resonant current with a fixed switching frequency and near 32% higher output power than that provided by traditional FM control methods under the same peak resonant current and peak voltage of v_{dc} .

5) The maximal efficiency of the buck converter is 98.7% with SiC MOSFETs and synchronous rectifier control, and the efficiency of the HBSRC for copper pan is 69.7% at 93 °C.

REFERENCES

- [1] *Cooktop Comparison: Gas, Electric and Induction*. [Online]. Available: <https://www.bijlibachao.com/appliances/cooktop-comparison-gas-electric-and-induction.html>
- [2] *What is Induction?* [Online]. Available: <http://www.sarvotech.com/induction.html>
- [3] B. Church and G. Winckles, "Assessing the safety of gas installations in buildings," *J. Building Appraisal*, vol. 2, pp. 86–94, Mar. 2006.
- [4] J. Acero, J. M. Burdio, L. A. Barragan, D. Navarro, R. Alonso, J. R. Garcia, F. Monterde, P. Hernandez, S. Llorente, and I. Garde, "The domestic induction heating appliance: An overview of recent research," in *Proc. 23rd Annu. IEEE Appl. Power Electron. Conf. Expo.*, Austin, TX, USA, Feb. 2008, pp. 651–657.
- [5] M. Pérez-Tarragona, H. Sarnago, Ó. Lucía and J. M. Burdío, "Active power factor corrector for high power domestic induction heating appliances," in *Proc. IECON-43rd Annu. Conf. IEEE Ind. Electron. Soc.*, Beijing, China, Oct. 2017, pp. 3779–3784.
- [6] O. Lucia, J. Acero, C. Carretero, and J. M. Burdio, "Induction heating appliances: Toward more flexible cooking surfaces," *IEEE Ind. Electron. Mag.*, vol. 7, no. 3, pp. 35–47, Sep. 2013.
- [7] J. Acero, C. Carretero, R. Alonso, and J. M. Burdio, "Quantitative evaluation of induction efficiency in domestic induction heating applications," *IEEE Trans. Magn.*, vol. 49, no. 4, pp. 1382–1389, Apr. 2013.
- [8] J. Acero, I. Lope, J. M. Burdio, C. Carretero, and R. Alonso, "Performance evaluation of graphite thin slabs for induction heating domestic applications," *IEEE Trans. Ind. Appl.*, vol. 51, no. 3, pp. 2398–2404, May 2015.
- [9] H. Kurose, D. Miyagi, N. Takahashi, N. Uchida, and K. Kawanaka, "3-D eddy current analysis of induction heating apparatus considering heat emission, heat conduction, and temperature dependence of magnetic characteristics," *IEEE Trans. Magn.*, vol. 45, no. 3, pp. 1847–1850, Mar. 2009.
- [10] J. Acero, J. M. Burdio, L. A. Barragan, J. I. Artigas, and R. Alonso, "An electromagnetic-based model for calculating the efficiency in domestic induction heating appliances," in *Proc. 37th IEEE Power Electron. Spec. Conf.*, Jeju, South Korea, June. 2006, pp. 1–6.
- [11] C. Carretero, R. Alonso, and J. Acero, "Interference emission estimation of domestic induction cookers based on finite-element simulation," *IEEE Trans. Electromagn. Compat.*, vol. 58, no. 4, pp. 993–999, Aug. 2016.
- [12] P. Viriya, S. Sittichok, and K. Matsuse, "Analysis of high-frequency induction cooker with variable frequency power control," in *Proc. Power Convars. Conf.-Osaka*, Osaka, Japan, Apr. 2002, pp. 1502–1507.
- [13] A. Dominguez, L. A. Barragan, A. Otin, D. Navarro, and D. Puyal, "Inverse-based power control in domestic induction-heating applications," *IEEE Trans. Ind. Electron.*, vol. 61, no. 5, pp. 2612–2621, May 2014.
- [14] O. Lucia, J. M. Burdio, I. Millan, J. Acero, and D. Puyal, "Load-adaptive control algorithm of half-bridge series resonant inverter for domestic induction heating," *IEEE Trans. Ind. Electron.*, vol. 56, no. 8, pp. 3106–3116, Aug. 2009.
- [15] A. Amrhein, "Induction heating of aluminum cookware," M.S. thesis, Elect. Eng., Virginia Tech., Blacksburg, VA, USA, 2015.
- [16] S. Villacís, J. Martínez, A. J. Riofrío, D. F. Carrión, M. A. Orozco, and D. Vaca, "Energy efficiency analysis of different materials for cookware commonly used in induction cookers," *Energy Procedia*, vol. 75, pp. 925–930, Aug. 2015.
- [17] *Panasonic Takes Induction to the Next Level*. [Online]. Available: <https://www.mountainhighappliance.com/cooking/cooktops/electric-cooktops/KYMK3500/>
- [18] W. Han, K. T. Chau, Z. Zhang, and C. Jiang, "Single-source multiple-coil homogeneous induction heating," *IEEE Trans. Magn.*, vol. 53, no. 11, pp. 1–6, Nov. 2017.

- [19] W. Han, K. T. Chau, and Z. Zhang, "Flexible induction heating using magnetic resonant coupling," *IEEE Trans. Ind. Electron.*, vol. 64, no. 3, pp. 1982–1992, Mar. 2017.
- [20] H.-P. Park, M. Kim, J.-H. Jung, and H.-S. Kim, "Load adaptive modulation method for all-metal induction heating application," in *Proc. IEEE Appl. Power Electron. Conf. Expo. (APEC)*, San Antonio, TX, USA, Mar. 2018, pp. 3486–3490.
- [21] I. Millán, J. M. Burdío, J. Acero, O. Lucía, and S. Llorente, "Series resonant inverter with selective harmonic operation applied to all-metal domestic induction heating," *IET Power Electron.*, vol. 4, no. 5, pp. 587–592, May 2011.
- [22] T. Hirokawa, E. Hiraki, T. Tanaka, M. Okamoto, and M. Nakaoka, "The practical evaluations of time-sharing high-frequency resonant soft-switching inverter for all metal IH cooking appliances," in *Proc. IECON-38th Annu. Conf. IEEE Ind. Electron. Soc.*, Montreal, QC, Canada, Oct. 2012, pp. 3302–3307.
- [23] N. Tsopelas and N. J. Siakavellas, "Influence of some parameters on the effectiveness of induction heating," *IEEE Trans. Magn.*, vol. 44, no. 12, pp. 4711–4720, Dec. 2008.
- [24] A. Amrhein and J.-S.-J. Lai, "A transformer-coupled, series-resonant topology for the induction heating of aluminum cookware," in *Proc. 9th Int. Conf. Power Electron. ECCE Asia (ICPE-ECCE Asia)*, Seoul, South Korea, Jun. 2015, pp. 1234–1239.
- [25] *IEC Industry standard*. [Online]. Available: https://en.wikipedia.org/wiki/IEC_61000-3-2
- [26] A. Roskopf, E. Bar, C. Joffe, and C. Bonse, "Calculation of power losses in Litz wire systems by coupling FEM and PEEC method," *IEEE Trans. Power Electron.*, vol. 31, no. 9, pp. 6442–6449, Sep. 2016.
- [27] S. Hiruma, Y. Otomo, and H. Igarashi, "Eddy current analysis of Litz wire using homogenization-based FEM in conjunction with integral equation," *IEEE Trans. Magn.*, vol. 54, no. 3, pp. 1–4, Mar. 2018.
- [28] J. Acero, R. Alonso, J. M. Burdío, L. A. Barragan, and D. Puyal, "Frequency-dependent resistance in Litz-wire planar windings for domestic induction heating appliances," *IEEE Trans. Power Electron.*, vol. 21, no. 4, pp. 856–866, Jul. 2006, doi: 10.1109/TPEL.2006.876894.



CHIH-CHIA LIAO (Graduate Student Member, IEEE) received the B.S. degree in electrical engineering from the National Taipei University of Technology, Taipei, Taiwan, in 2014, where he is currently pursuing the Ph.D. degree. His research interests include bidirectional AC–DC/DC–DC converter, wireless power transfer, resonant converter, energy storage systems, power electronics, and digital control.



ZHENG-FENG LI (Graduate Student Member, IEEE) received the B.S. and M.S. degrees in electrical engineering from the National Taipei University of Technology, Taipei, Taiwan, in 2015 and 2017, respectively, where he is currently pursuing the Ph.D. degree. His research interests include resonant converter, wireless power transfer, motor design, and digital control.



ZHI-REN SHIH received the B.S. and M.S. degrees in electrical engineering from the National Taipei University of Technology, Taiwan, in 2016 and 2018, respectively. His research interests include resonant converter and digital control.



MING-SHI HUANG (Member, IEEE) received the B.S. degree in electrical engineering from the National Taiwan University of Science and Technology, Taiwan, in 1987, the M.S. degree in electrical engineering from Tatung University, Taiwan, in 1991, and the Ph.D. degree in electrical engineering from National Tsing Hua University, Taiwan, in 2004. From 1987 to 2004, he was a Researcher with the Mechanical Industry Research Laboratories, Industrial Technology Research Institute. He is currently a Professor with the Department of Electrical Engineering, National Taipei University of Technology, Taipei, Taiwan. His areas of research interests include power electronics, variable-speed drives, and electrical power train in vehicle applications.



HSIU-WEN HSUEH received the master's degree in business administration from the National Changchun University of Education, Taiwan, in 2013. She is currently pursuing the Ph.D. degree with the Department of Industrial Education and Technology, National Changhua University of Education, Taiwan. Her research interests include engineering technology, financial technology, service science, air-pollution forecasting, and control using AI.

...